Polarization of actin cytoskeleton is reduced in dendritic protrusions during early spine development in hippocampal neuron

Vedakumar Tatavarty*, Sulagna Das*, and Ji Yu
Center for Cell Analysis and Modeling, University of Connecticut Health Center, Farmington, CT 06030

ABSTRACT Dendritic spines are small protrusions that receive synaptic signals in neuronal networks. The actin cytoskeleton plays a key role in regulating spine morphogenesis, as well as in the function of synapses. Here we report the first quantitative measurement of F-actin retrograde flow rate in dendritic filopodia, the precursor of dendritic spines, and in newly formed spines, using a technique based on photoactivation localization microscopy. We found a fast F-actin retrograde flow in the dendritic filopodia but not in the spine necks. The quantification of F-actin flow rates, combined with fluorescence recovery after photobleaching measurements, allowed for a full quantification of spatially resolved kinetic rates of actin turnover, which was not previously feasible. Furthermore we provide evidences that myosin II regulates the actin flow in dendritic filopodia and translocates from the base to the tip of the protrusion upon spine formation. Rac1 inhibition led to mislocalization of myosin II, as well as to disruption of the F-actin flow. These results provide advances in the quantitative understanding of F-actin remodeling during spine formation.

INTRODUCTION

Normal brain function depends crucially on tiny structures known as dendritic spines. The spines protrude from dendritic shafts and are believed to compartmentalize postsynaptic molecules (Nimchinsky *et al.*, 2002). Mature dendritic spines are usually mushroom shaped with an enlarged head and a thin neck that connects to the dendritic shaft. Other varieties of shapes also exist (Harris *et al.*, 1992; Arellano, 2007); for example, "thin spines" have a pronounced neck region but a smaller head region, and the "stubby spines" are spines without an obvious neck region. Dendritic spines are believed to derive from dendritic filopodia, which are thin, elongated dendritic protrusions that are most commonly observed in the early developmental stages of the neuron (Segal, 1995; Ziv and Smith, 1996; Ethell and Pasquale, 2005). The morphology of these dendritic protrusions has garnered attention owing to findings that biological attributes of synapses are impacted by changes in spine morphology (Yuste and Bonhoeffer, 2001). Morphological abnormalities in dendritic spines are in fact linked to diseases of mental retardation such as the fragile X syndrome (Irwin *et al.*, 2000; Calabrese *et al.*, 2006), underscoring the importance of spine morphology in cognition. Both the dendritic spines and the dendritic filopodia use a dynamic network of actin to generate protrusions (Hotulainen and Hoogenraad, 2010). The actin cytoskeleton is hence believed to play an important role in regulating spine morphology and, consequently, synaptic function (Ethell and Pasquale, 2005; Cingolani and Goda, 2008).

Actin cytoskeleton in cellular protrusions (e.g., lamellipodia and filopodia) is typically highly polarized. In the lamellipodia of motile cells, for example, actin cytoskeleton is organized into an ordered dendritic network of filaments (Pollard and Borisy, 2003). Factors that promote actin nucleation, such as N-WASP and WAVE, are activated at the leading edge of the migrating cell (Kawamura *et al.*, 2004; Ward *et al.*, 2004), resulting in a net polymerization of actin (i.e., the rate of polymerization is greater than the rate of

depolymerization) at the leading edge. The growth of the actin network pushes the plasma membrane, and the membrane exerts a counterforce that moves actin filaments away from the edge, resulting in a unidirectional flow called retrograde flow (Theriot and Mitchison, 1992; Lin et al., 1994). Thus the polarization of the actin network is manifested in both the structure and the dynamics. In neurons, the polarity of actin cytoskeleton in the spine head has attracted interests from various groups. Immunogold electron microscopy (EM), for example, has shown that actin regulatory factors are sometimes nonuniformly localized in the spine heads: cortactin (Racz and Weinberg, 2004) and profilin (Neuhoff et al., 2004) are found to concentrate near the center of the spine head, whereas cofilin lies near the plasma membrane (Racz and Weinberg, 2006). Furthermore, actin dynamics in spine heads has been studied in live cells by either fluorescence redistribution assays (Honkura et al., 2008) or single-molecule tracking (Tatavarty et al., 2009; Frost et al., 2010). In comparison, less is known about the actin polarization in the dendritic filopodia or in the spine necks. EM of actin filaments (Korobova and Svitkina, 2010) in dendritic filopodia showed branched filaments, a feature indicative of Arp2/3-dependent nucleation. Of interest, filaments of opposite polarity were detected (Korobova and Svitkina, 2010), suggesting a more complicated picture of the polarity. Little is known about the dynamics of F-actin in the dendritic filopodia or in the spine necks.

To further our understanding of the mechanisms underlying spine morphogenesis, it is important to understand actin dynamics in dendritic protrusions at different stages of development. A major hurdle, however, has been that the small dendritic protrusions cannot be easily resolved by optical microscopy. Recently a new assay that uses photoactivation localization microscopy (PALM) demonstrated subdiffractional resolution of single-molecule tracking in live cells (Manley et al., 2008; Niu and Yu, 2008). This technique was then used to analyze F-actin's kinematic flows in mature spine heads (Tatavarty et al., 2009; Frost et al., 2010). In this study, we applied the PALM technique to analyze actin dynamics during the early stages of spine morphogenesis. Specifically, we compared the dynamics of the actin cytoskeleton in the dendritic filopodia, which are highly motile, with young spines, which are stabilized upon spinogenesis. Our results shed light on the complex rearrangement of the actin cytoskeleton that occurs in concert with spinogenesis.

RESULTS

Retrograde flow of F-actin in dendritic protrusions

To monitor early spine formation, we used embryonic rat hippocampal neuron cultures. Cells were seeded at medium to low density, which facilitated the direct observation of dendritic morphology and cell-to-cell contacts under differential interference contrast (DIC). Cultured pyramidal neurons produced dendritic protrusions with distinct stages of morphological progression that is characteristic of this model system (Takahashi et al., 2003; Oray et al., 2006). Dendritic filopodia could be observed as early as 6 d in vitro (DIV) and became abundant around DIV 9, reaching a density of 0.27 ± 0.10 μm⁻¹. By DIV 14, the dominant dendritic protrusions are thin spines, characterized by a relatively long neck (average length, 1.78 μm) and a small head (<1 μm in size). Mature, mushroom-shaped spines became abundant at about DIV 18–21.

Cells were transfected with a DNA vector expressing Eos-actin fusion protein. Time-lapse videos were recorded through an orange fluorescence filter set, which detects photoactivated Eos molecules for cells at DIV 9–10 (Supplemental Videos S1 and S2) to study dendritic filopodia (Figure 1A) and for cells at DIV 13–14 (Supplemental Videos S3 and S4) to study early spines (Figure 1B). Single molecules

of Eos-actin can be detected in both conditions (Figure 1C). The images of actin molecules appear as diffraction-limited spots, as expected from single molecules. The fluorescence signal of the molecules sometimes disappears abruptly and then recovers after one or more imaging frames (Figure 1C). This is typical of single-molecule fluorescence and is caused by the formation of metastable photophysical dark states (Dickson et al., 1997).

The direction of the actin kinematic flow can be easily discerned from the kymographs of the fluorescence signal from the protrusions (Figure 1D). In the kymographs, the signal from single F-actin molecules appears as bright lines. The lines stop abruptly, most likely due to photobleaching of the chromophore. Intensities of the molecules varied because some molecules are positioned slightly off the scan line of the kymograph. G-actin molecules are also detected occasionally. However, because they diffused out of the dendritic protrusions very quickly, they appear as dots in the kymograph instead of continuous lines. In the dendritic filopodia, almost without exception, the flow of F-actin molecules is in the retrograde direction (yellow arrowheads in Figure 1D). The speed varies from molecule to molecule and sometimes for the same molecule at different time periods, demonstrated by varying slopes of the kymographic lines. In contrast, in the spine necks, many molecules showed no discernible movement (Figure 1D). Furthermore, for molecules that exhibited significant directional motions, the flow direction could be either in the retrograde direction (Figure 1D, yellow arrowhead) or in the anterograde direction (Figure 1D, blue arrowhead).

To quantify the F-actin flow pattern, we measured the distributions of retrograde flow rates of individual F-actin molecules that were tracked for at least 6 s (Figure 2, A and B) for time-lapse data taken at 1 frame/s and 10 s for data taken at one frame every 2 s. Molecules that were tracked for shorter duration were not analyzed due to larger errors in the measurements. The sign convention of the retrograde flow rate was that a negative sign represented an anterograde flow. The average retrograde flow rate in dendritic filopodia, based on the analysis of 314 molecules from eight different experiments, was 1.20 μm/min. Variations of retrograde flow rates from molecule to molecule were large, as can be seen from the width of the distribution (Figure 2A). A Gaussian fit of the distribution gave a full-width at half-maximum (FWHM) of 0.97 μm/min. In contrast, the average retrograde flow rate of F-actin in the spine necks, based on analysis of 260 molecules from six experiments, was 0.033 μm/min, which is more than an order of magnitude lower than in dendritic filopodia (Figure 2C). In addition, the distribution plot of the flow rates in spine neck showed that the variation between the molecules is less significant compared with dendritic filopodia, with a FWHM of 0.51 μm/min (Figure 2B). It should be noted that due to the finite resolution of PALM (~30 nm), each flow-rate measurement was associated with a measurement error on the order of 0.18 μm/min (i.e., 30-nm displacement over a 10-s single-molecule trace). Therefore for thin spines, a large part of the flow rate distribution width could be attributed to the measurement noise and not the real variations of the flow rates. Finally, we also compared the absolute speed of F-actin molecules regardless of the flowing direction (Figure 2D). This result shows that F-actin molecules in dendritic spine necks are moving more slowly than molecules in dendritic filopodia.

To evaluate whether retrograde flow rates varied spatially along the lengths of the dendritic protrusion, we grouped individual molecules based on their distance from the dendritic shaft and calculated the average F-actin flow rates as a function of the distance (Figure 2, E and F). We found little variation of the retrograde flow rate along the protrusion length. However, near the base of the
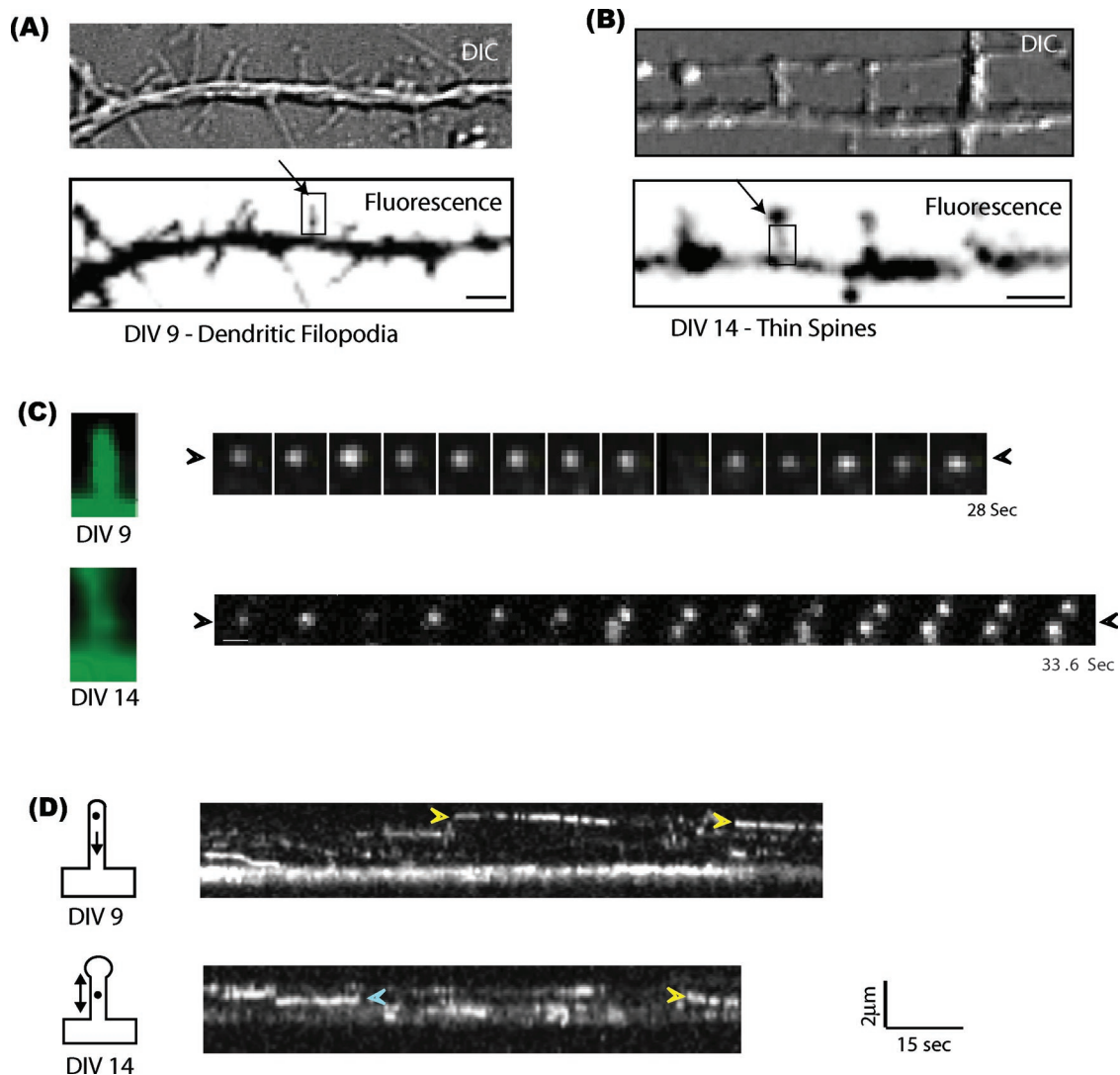
FIGURE 1: Kinematic flow of F-actin in dendritic protrusions. (A, B) DIC (top) and fluorescence (bottom) images of a dendritic segment of a neuron. Both the DIC and fluorescence images indicated dendritic filopodia at DIV 9 (A) and thin-spine formation (B) at DIV 14. Scale bar, 2 μm. (C) Time-lapse fluorescence image series of single Eos-actin molecules, each from either the dendritic filopodia or the thin spine denoted by the box and arrow in A and B. The small arrows on both sides of the image denote the centroid position of the molecule from the first frame. In filopodia, the molecule moved downward toward the dendrite (retrograde), whereas in thin spines, one of the two molecules moved away from the dendrite (anterograde) and the other remained stationary. Scale bar, 1 μm. (D) Kymographs of Eos-actin signal in the dendritic protrusions. The yellow arrowheads denote the retrograde motion of a single Eos-actin molecule, whereas the blue arrowheads show the anterograde motion.

filopodia (i.e., close to the dendritic shaft), the rate decreases to about half of the peak value (Figure 2E). Similar measurements in the spine necks (Figure 2F) showed no significant variations.

Net actin polymerization rate in dendritic protrusions
One signature characteristic of the polarized actin cytoskeleton is the imbalance of local polymerization rate and the depolymerization rate, resulting in net polymerization of F-actin in certain regions and net depolymerization in others. To test whether this is the case for early dendritic protrusions, we carried out fluorescence recovery after photobleaching (FRAP) experiments in dendritic filopodia and in the spine necks (Figure 3, A and B). Both structures exhibited significant fraction of fluorescence recovery: $78 \pm 4\%$ in dendritic filopodia and $72 \pm 4\%$ in the thin spine neck. The average characteristic recovery time, obtained by fitting the overall fluorescence recovery with a single-exponential function, is 49.2 s for dendritic

filopodia ($n = 9$) and 36.6 s for the spine neck ($n = 6$). These recovery times are on the same time scale as that of the spine head (Star *et al.*, 2002; Honkura *et al.*, 2008), indicating that uncapped dynamic actin filaments exist in all these dendritic protrusions. Furthermore, in dendritic filopodia, the fluorescence recovery speed was different for different subregions, consistent with a previous study (Hotulainen *et al.*, 2009). The tip had the fastest fluorescence recovery rate, followed by the base, and the middle part of the filopodia was the slowest (Figure 3, A and C). This differential recovery pattern was not observed for spine necks (Figure 3, B and D).

To quantify the kinetic rates of actin polymerization and depolymerization, it is important to recognize that the fluorescence recovery in the FRAP experiment is due to a combination of kinematic flow of filaments, as well as the kinetic turnover of the actin units. The former replaces F-actin at one location with F-actin from an adjacent region, and the latter replaces the existing F-actin
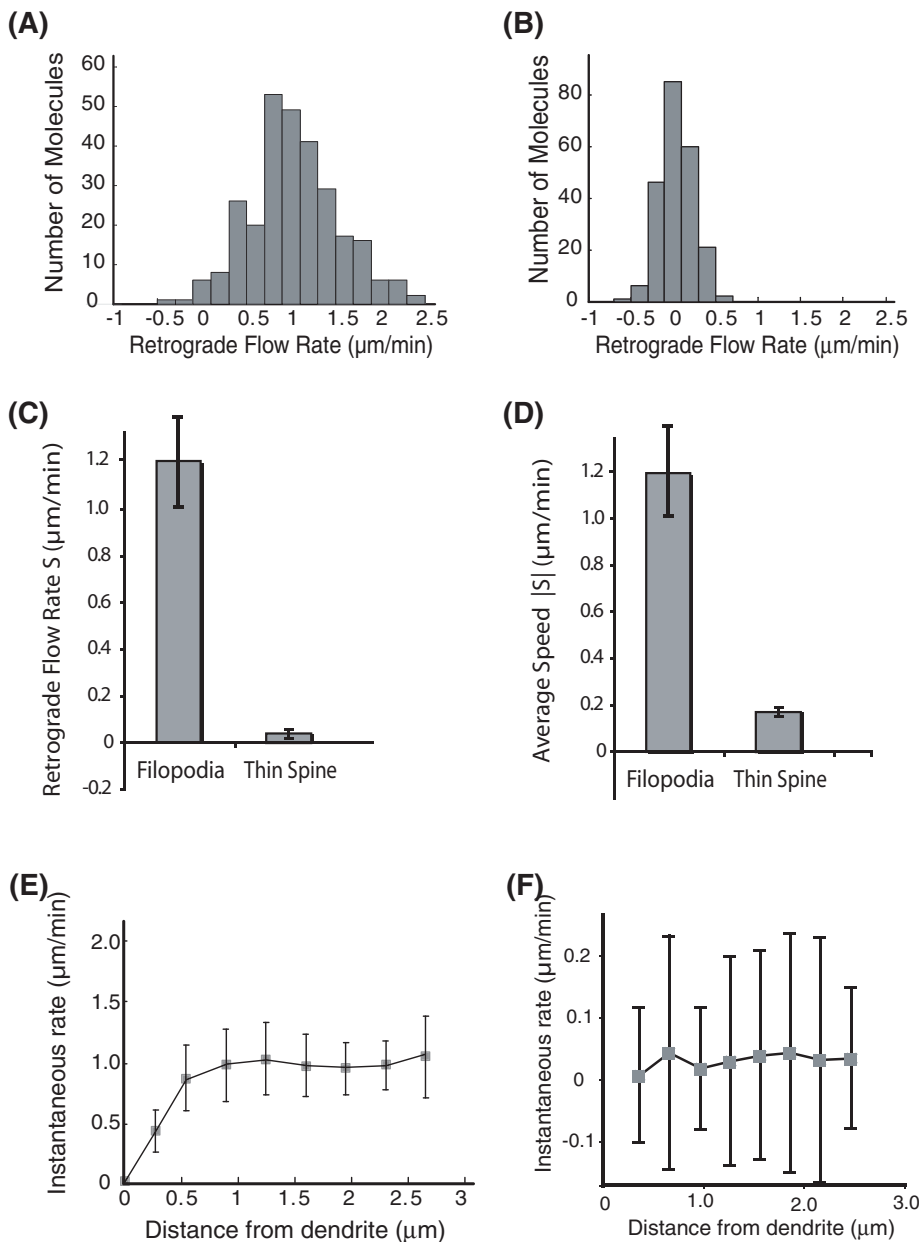
FIGURE 2: Analysis of the F-actin retrograde flow rates. (A) Distribution of the retrograde flow rates of individual F-actin molecules detected in the dendritic filopodia (89 filopodia from eight experiments) (B) Distribution of the retrograde flow rates of individual F-actin molecules detected in the neck regions of the thin spines (60 spine necks from six experiments). A negative value in either A or B indicates the anterograde direction. (C, D) Comparison of the average retrograde flow rate (C) or the average flow speed in either direction (D) between the filopodia and the thin spines. The error bars denote variation (SEM) from different experiments. (E, F) The retrograde flow rate of F-actin molecules as a function of the molecule distances from the dendritic shaft. The results for the dendritic filopodia (46 filopodia from four experiments) are shown in E, and the results from the thin spines (35 thin spines from four experiments) are shown in F. The retrograde flow rates were averaged for each 300-nm segment. The size of the error bar represents the SD of the flow rates from different dendritic filopodia. The calculation was cut off at 3 μm from the base, even though some dendritic filopodia could be longer than that.

molecules with newly polymerized G-actin. A general equation that encompasses both components is

$$\frac{\partial C(x,t)}{\partial t} = R_+(x) - R_-(x)\frac{C(x,t)}{C_0(x)} - \frac{\partial v(x)C(x,t)}{\partial x} \qquad (1)$$

where $C(x, t)$ is the concentration of fluorescent F-actin at location x and can be measured with a FRAP experiment, $v(x)$ is the retrograde flow rate, $C_0(x)$ is the overall (fluorescent plus bleached) concentration of F-actin, and $R_+(x)$ and $R_-(x)$ are the polymerization depolymerization rates, respectively (not rate constants). Because we had already measured the flow rate $v(x)$ with PALM, we could quantify R_+ and R_- by modeling the FRAP results with the foregoing equation. The quantifications are shown in Figure 3E. As expected, we found that the local polymerization and depolymerization rates are unbalanced in dendritic filopodia but are mostly balanced in spine necks. The tips of dendritic filopodia had the highest polymerization rates, followed by the bases. The polymerization rate and the depolymerization rate at the middle part of the dendritic filopodia are small but significantly greater than zero.

Myosin II activity regulates the retrograde F-actin flow

Next we tested whether the force applied by motor proteins played a role in controlling the kinematic flow of F-actin and actin dynamics. We evaluated the effects of the myosin II by chemically blocking myosin II activity and remeasuring the F-actin flow rate in dendritic filopodia. To inhibit myosin II activity, we treated cells with myosin light-chain kinase inhibitor ML7 (Makishima *et al.*, 1991). We found the treatment inhibit the retrograde flow of F-actin in treated cells (Figure 4, A–C, and Supplemental Video S5). Many actin molecules in treated cells were stationary. The average retrograde flow rate was reduced to 0.15 μm/min. We also attempted to inhibit myosin with the myosin II heavy chain inhibitor blebbistatin. Unfortunately, blebbistatin has a strong absorption in the blue/green range of the spectrum and emits a weak fluorescence signal that partially overlaps with the Eos fluorescence. This overwhelms the weak single-molecule signal emanating from Eos-Actin. Therefore, instead of measuring the retrograde flow in the presence of blebbistatin, we opted to make the measurement immediately after the washout of the drug after a short period of treatment (10 min). We found that under this condition, the average retrograde flow rate was reduced but not completely abolished (0.43 μm/min; see Figure 4, A and C, and Supplemental Video S6). Thus inhibition of either the light chain or the heavy chain of myosin II significantly reduced the retrograde F-actin flow rate in filopodia.
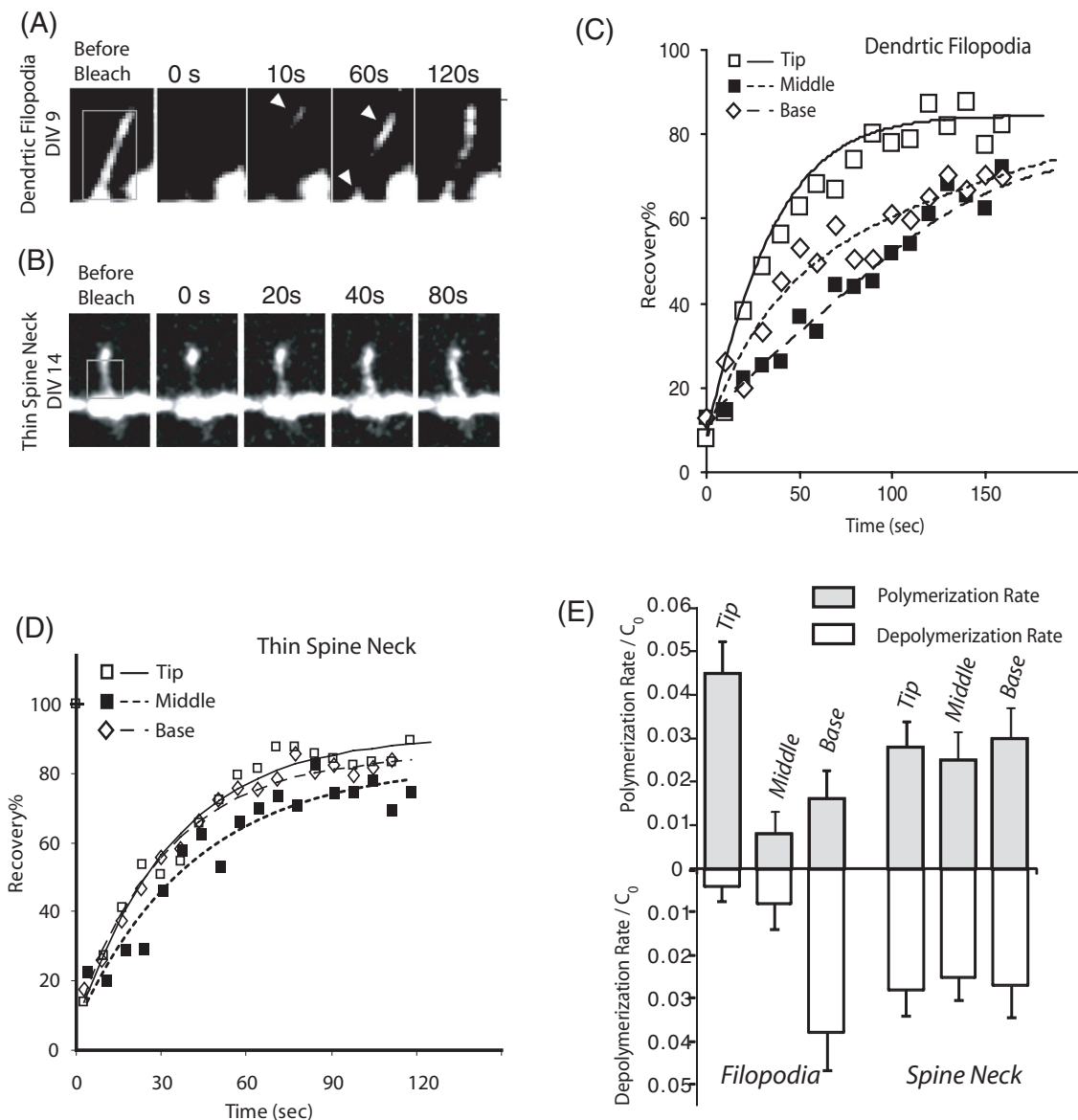
FIGURE 3: Quantification of actin polymerization and depolymerization rates. (A) FRAP of Eos-actin in a dendritic filopodium from a DIV 9 neuron. (B) FRAP of Eos-actin in the neck region of a thin spine from a DIV 14 neuron. The boxes denote the region of photobleaching. (C, D) Normalized fluorescence signal from the tip, the shaft, and the base of the dendritic filopodium (C) and the thin spines (D). The symbols represent experimental data. The lines represent computational results based on Eq. 1 (see the text). (E) The average polymerization and depolymerization rates in subregions of the dendritic filopodia ($n = 5$) and the spine necks ($n = 3$). Average values were calculated for the tip, the middle point, and the base regions. All rates were normalized to total actin concentration C_0.

Myosin II activity promotes dendritic filopodia motility

Next we tested whether myosin II activity affected the motility of the dendritic filopodia. We transfected cells with a myristoylated variant of green fluorescent protein (MyrGFP), which labels the cell membrane. The position of the tip of the filopodia was tracked in time with fluorescence time-lapse microscopy (Figure 4D and Supplemental Video S7), and the amount of tip movement was calculated for every 2 min (Figure 4E). We found that the inhibition of myosin II by blebbistatin significantly reduced but did not completely inhibit the motility (Figure 4, D and E). As a comparison, blocking actin polymerization by cytochalasin D completely inhibits the filopodia motility (Supplemental Video S8), suggesting that actin polymerization is the main factor in controlling the filopodia dynamics, whereas myosin II plays a regulatory role.

Distribution of active myosin II in dendritic protrusions

Next we carried out immunofluorescence microscopy using an antibody against the phosphorylated form of the regulatory myosin light chain (pMLC) to investigate the localization of myosin II activity (Figure 5A). For neurons at DIV 7–8, pMLC was rarely detected in the dendritic protrusions, but it was detected at the base of most of the filopodia-type protrusions (Figure 5B). However, with increasing DIV, myosin II immunoreactivity was detected increasingly along the protrusions. For neurons at DIV 16 (Figure 5A), we detected strong pMLC immunoreactivity at the tip/head of the spines but no significant signal in the stem of the spine necks. Overall, the localization of the pMLC gradually shifted from the base to the head during the transition from the filopodia to the spine stage (Figure 5B).
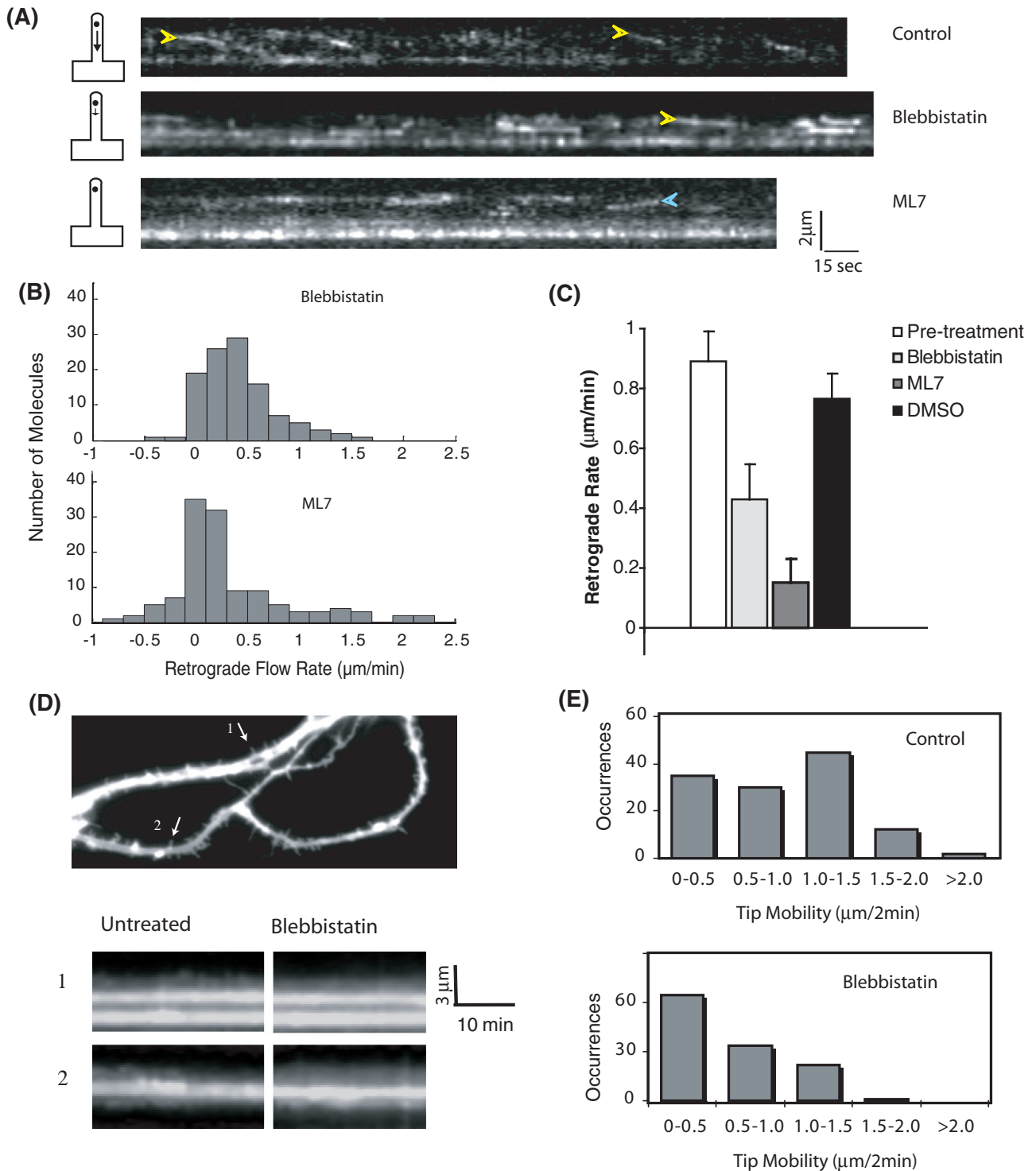
FIGURE 4: Regulation of dendritic filopodia dynamics by myosin II. (A) Kymographs of Eos-actin from control (top), blebbistatin-treated (middle), and ML7–treated (bottom) neurons at DIV 7–9. In blebbistatin-treated cells, the images were acquired after the washout of the drug. Yellow arrowheads indicate the retrograde flow; the blue arrowheads indicated the anterograde flow. (B) Distribution of the retrograde flow rates of individual F-actin molecules detected in the dendritic filopodia treated with blebbistatin (41 filopodia) and ML7 (33 filopodia). (C) Comparison of the average retrograde flow rates. The error bars denote SEM. (D) Kymographs (bottom) of the MyrGFP fluorescence in two filopodia (indicated by the arrows in the top image) from the dendritic segment of a DIV 9 neuron. Images were taken with 1-min time delay. (E) Quantification of the tip mobility of the filopodia (*n* = 48) before and after blebbistatin treatment. Movements of the tip were calculated every 2 min.
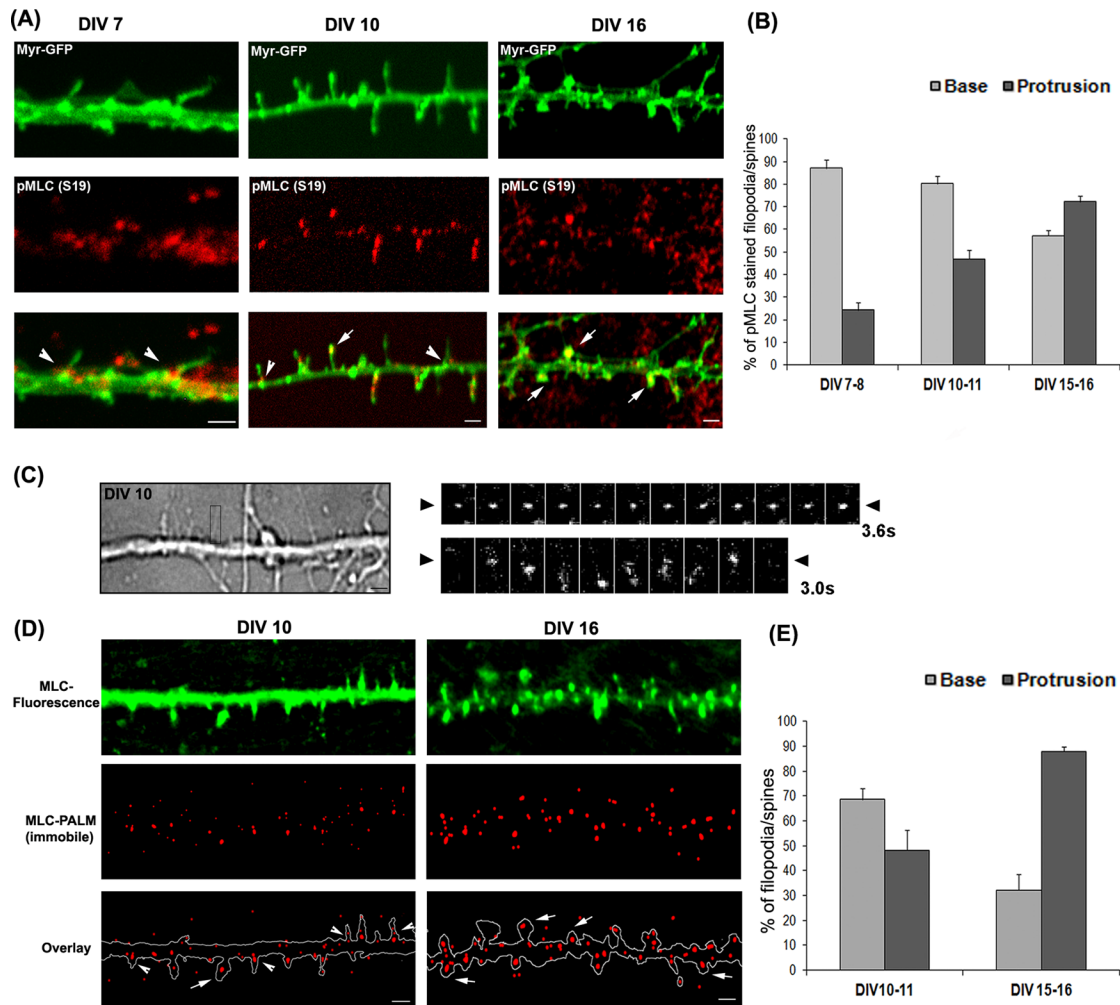
FIGURE 5: Localization of myosin II in dendritic protrusions. (A) Localization of pMLC. Hippocampal neurons were transfected with MyrGFP (green) and then stained for phosphorylated (Ser-19) myosin regulatory light-chain (pMLC) antibody labeled with Alexa 647 (red). Active myosin localization to the triangular base of the filopodia protrusions is shown by arrowheads, and that in the spine heads is denoted by arrows. Scale bar, 2 μm. (B) Quantification of pMLC localization for neurons at DIV 7–8 ($n = 70$), 10–11 ($n = 81$), and 15–16 ($n = 98$). Gray bars denote percentage protrusions with pMLC localized at the base, and black bars denote percentage of protrusions with pMLC localized along the protrusion shaft or in the tip. (C) Examples of single-molecule traces from PALM imaging of Eos-MLC. Both the immobile (top right) and the mobile (bottom right) molecules were detected from the dendritic filopodia protrusion (denoted by the box in the bright-field image on the left). (D) Localization of MLC based on PALM imaging. Top, epifluorescence images of neurons transfected with Eos-MLC. Middle, corresponding PALM images constructed with only the immobile subpopulation of the molecules (see the text for details). Bottom, the overlay. Arrowheads indicate immobile MLC localization in the base of the filopodia. Arrows indicate immobile MLC localization in the spine heads. Scale bar, μm. (E) Quantification of immobile MLC localization based on PALM images of neurons at DIV 10–11 ($n = 36$) and 14–15 ($n = 45$). Errors bars represent SEM from different experiments.

To verify the immunofluorescence results, we also expressed fusion of Eos with regulatory myosin light chain (Eos-MLC) in neurons. Although the epifluorescence microscopy did not immediately show a polar localization in dendritic protrusions, we noticed that when we imaged the single molecules with PALM, some molecules were stationary, whereas others were highly mobile (Figure 5C). Because active pMLC is associated with the actin filaments, we speculated that the stationary molecules represented the active population. Therefore we generated PALM images using the positions of only the stationary molecules (Figure 5D), which showed preferred localization at the base of the dendritic filopodia, and at the head of the early spines (Figure 5E). Furthermore, in young neurons, patches of

immobile MLC molecules can sometimes be found at the dendritic shaft without a corresponding filopodial protrusion. The localization pattern does not simply follow the F-actin concentration, indicating that the localization is regulated by other factors.

Inhibiting Rac1 disrupts actin polarization in dendritic filopodia

A well-characterized neuronal phenotype is that dominant-negative Rac1expression leads to elongated dendritic filopodia and negatively affects spine formation (Tashiro and Yuste, 2004). Rac1 is known to regulate myosin light-chain kinase in hippocampal neurons (Zhang et al., 2005). Thus we suspect that one of the consequences of
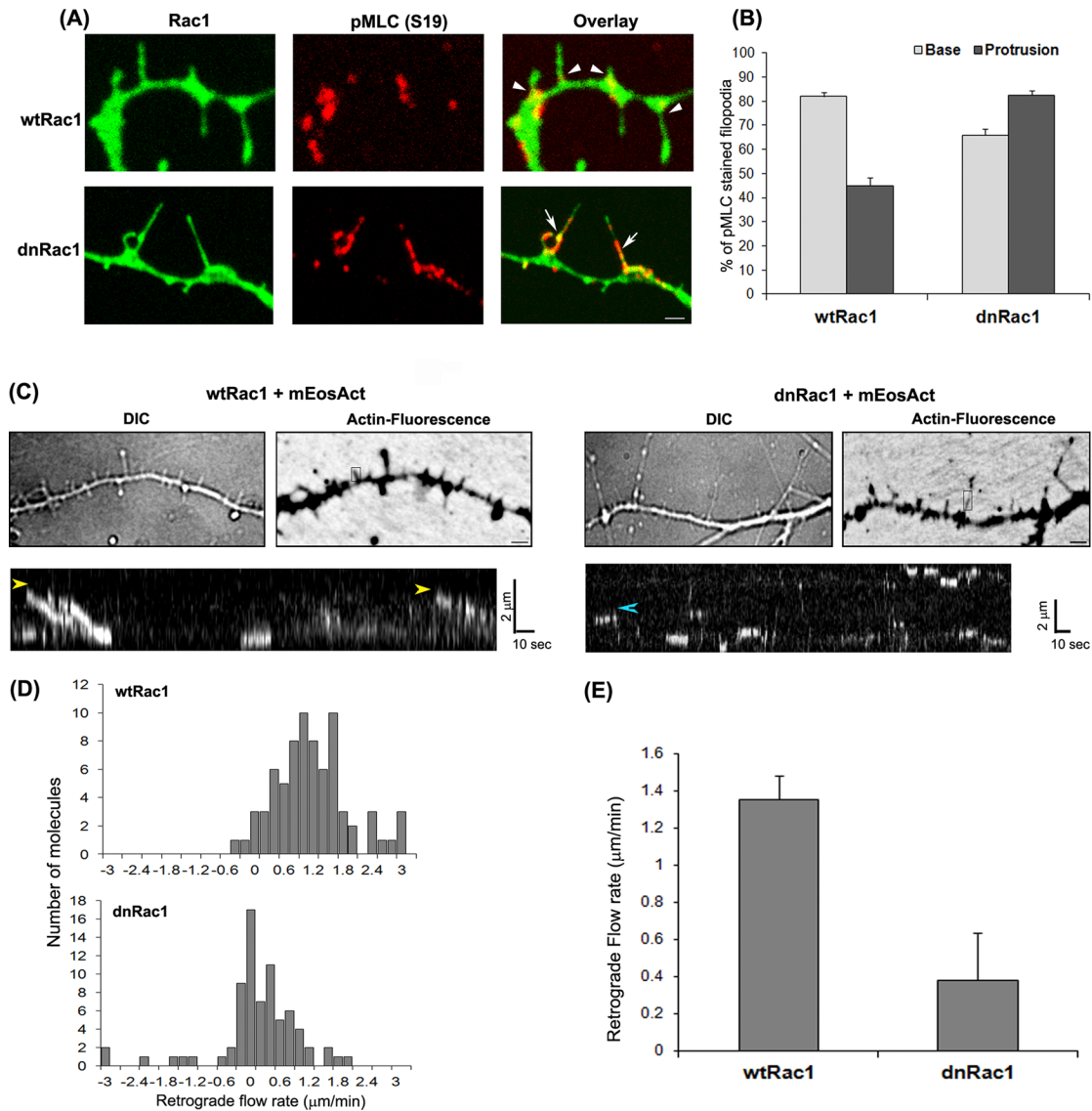
FIGURE 6: Effect of Rac1 inhibition on actin polarization in dendritic filopodia. (A) The pMLC localization (red) in young hippocampal neurons (DIV 10) transfected with wtRac1-GFP (green) or dnRac1-GFP (green). Arrowheads indicate pMLC signal at the base of the filopodia, and arrows indicate pMLC signal within the stems of the filopodia-like protrusions. Scale bar, 2 μm. (B) Quantification of pMLC immunofluorescence in filopodia-like protrusions in wtRac1-expressing (n = 100) or dnRac1-expressing (n = 103) neurons. (C) F-actin retrograde flow in hippocampal neurons transfected with Rac constructs (wtRac1 or dnRac1) and Eos-actin. DIC and fluorescence images of a dendritic segment of a DIV 10 neuron (top) indicate short filopodia formation in wtRac1 and long filopodia-like protrusions in dnRac1-transfected cells. Kymographs of Eos-actin molecules (bottom) show different retrograde flow rates. (D) Distributions of the retrograde flow rates for wtRac1-expressing (31 filopodia) or dnRac1-expressing (38 filopodia) cells. (E) Comparison of average retrograde flow rates in control and dnRac1-transfected neurons at DIV10. All error bars denote SEM.

extended inhibition of Rac1 is the misregulation of F-actin polarization. To test this, we examined the pMLC localization in cells expressing dnRac1. We found that in these cells, pMLC is no longer confined to the base of the filopodia-like protrusions but is also found along the length of the protrusion (Figure 6, A and B). Furthermore, using live-cell PALM microscopy, we confirmed that there is essentially no F-actin net retrograde flow in these protrusions from dnRac1 cells (Figure 6, C–E, and Supplemental Video S9). In comparison, cells expressing wild-type Rac1 did not exhibit obvious defects in either the pMLC localization or F-actin retrograde flow dynamics (Figure 6, C–E, and Supplemental Video S10). Therefore, dnRac1 expression caused mislocalized myosin II activity and altered the kinematic flow of F-actin in dendritic filopodia.

DISCUSSION

F-actin polarization in dendritic filopodia and in spine necks

We investigated the actin dynamics in dendritic protrusions during the early developmental stages of spine formation using PALM and FRAP microscopy. The results from dendritic filopodia indicated a highly polarized actin network, as evidenced by the high F-actin retrograde flow rate, the net actin polymerization at the tip, the net delopolymerization at the base, and the polar localization of the myosin II. The polarization is presumably important for the spinogenesis. Disruption of the actin polarization in neurons, for example, by Rac1 inhibition, is correlated with defects in spine formation (Tashiro and Yuste, 2004). In comparison, spine necks exhibited a bidirectional F-actin flow, almost no net retrograde flow, and locally

balanced polymerization and depolymerization rates. Active myosin II was not confined to the base of spines but was also detected in the protrusion and was most abundant in the spine heads. Therefore we conclude that the actin cytoskeleton is less polarized in the spine necks, at least for thin spines of the early development stage.

Actin polarization is normally associated with membrane protrusional forces and cell motility, and the thin spine is a type of membrane protrusion that requires a protrusional force to maintain its shape. Thus our result raises the question of how the thin spine can maintain its shape without a highly polarized actin cytoskeleton. We can imagine three possibilities: First, the spines may contain a large amount of static F-actin that serves as a structural support. For example, it was proposed that the spine core and spine neck contain stable actin filaments, whereas the spine shell contains dynamic actin filaments (Halpain, 2000). This proposal, however, is not consistent with the fast FRAP recovery in the spine necks. The second possibility is that the protrusional force may be entirely due to the F-actin in the spine head. Recent evidence suggested that the F-actin in the spine head might be polarized (Frost et al., 2010). However, the polarization was believed to be symmetric around the center of the spine head (Frost et al., 2010), and therefore the net force on the spine head is probably close to zero. Third, the spine might rely on cell-to-cell and cell-to-matrix adhesion to maintain its shape. A variety of cell-to-cell adhesion molecules, such as N-cadherin and syndecan, were found to play important roles in synapse formation (Ethell and Pasquale, 2005) and may provide a mechanism for maintaining spine morphology after the formation of synaptic contacts. Furthermore, the dendritic filopodia were believed to form adhesion through telencephalin (TLCN)–ezrin/radixin/moesin (ERM) interaction with the actin cytoskeleton (Yoshihara et al., 2009). The adhesion might survive to early stage of the thin spines. We believe this last scenario to be the most plausible one among the three.

Quantification of the kinematic flow and the kinetic turnover

PALM imaging provided a unique way to investigate the kinematic flow of F-actin in a dynamic actin cytoskeleton (Tatavarty et al., 2009; Frost et al., 2010). It is important to recognize that even though only one molecule within a filament is imaged, the movement of the molecule is indicative of the same physical movement of the whole filament. Furthermore, the movement is a direct evidence of a force exerted on the filament and thus can be called a kinematic flow. In a low–Reynolds number condition, such as in the cell cytoplasm, the force is proportional to the velocity of the flow (Deshpande et al., 2008). On the other hand, kinetic processes, such as filament turnover, defined as the continuous extension of the barbed end and the accompanying shrinkage of the pointed end, does not automatically cause a kinematic flow unless the extension is against a fixed spatial point, such as the cell membrane, thus generating a physical force on the filament. Conversely, a kinematic flow could be observed for a capped static filament because the force could be exerted by another filament in a cross-linked actin network or by motor proteins such as myosin. In either case, the direction of the flow can also be different from the orientation of the filament. These mechanisms could also explain why a unidirectional flow was observed in dendritic filopodia despite the fact that the filaments are of mixed orientations (Korobova and Svitkina, 2010).

The flow of F-actin has also been investigated by other methods, such as fluorescence redistribution (Honkura et al., 2008). However, the F-actin flow observed in such an assay, in principle, is not purely kinematic but might also contain contributions from kinetic events, such as depolymerization of the F-actin molecules in one location

and reincorporation of the molecules to other filaments in a nearby region. The FRAP experiment is also a type of fluorescence redistribution assay and suffers from a similar caveat: the fluorescence recovery could be due to either kinematic flow of F-actin or F-actin polymerization and depolymerization. However, by combining PALM with FRAP, we could separately quantify the kinematic flow rate and the kinetic rates of polymerization and depolymerization, which provided more precise description of the actin dynamics. Specifically, we found the following, based on our calculation: 1) The actin polymerization occurs throughout the dendritic filopodia; however, the tip and the base have higher rates than the middle. 2) The depolymerization rate is highest at the base but is nonzero throughout the dendritic filopodia, including the middle part of the protrusion, indicating that there are uncapped pointed ends throughout the protrusion. This observation is consistent with the EM study (Korobova and Svitkina, 2010), which showed many short actin filaments throughout the filopodia. 3) In spine necks, polymerization/depolymerization also occurs throughout, but the rates do not vary spatially. 4) Unlike in dendritic filopodia, the polymerization rates and depolymerization rates are balanced everywhere in spine necks, resulting in no net polymerization or net depolymerization.

Myosin II and actin retrograde flow

In mature neurons, myosin II has been found to be active in the spine head and to play a critical role in synaptic plasticity (Ryu et al., 2006; Rex et al., 2010). The presence of myosin II in the dendritic filopodia was reported by an earlier study (Korobova and Svitkina, 2010), although its functional role was not elucidated. Here, we report the differential spatial localization of active myosin at different stages of spine development. We also attempted to discern the possible role of this motor in these structures and how its precise localization is important for control of actin dynamics. Myosin II has been extensively studied in various motile actin structures. In axon growth cones, for example, myosin II was found in the lamellipodia near the base of the filopodia actin bundles and accelerates the retrograde flow of the F-actin in the filopodia (Medeiros et al., 2006). Similar effects were found in our studies of the dendritic filopodia. An important distinction, however, is that in the axon growth cone, the filopodia contains bundled F-actin, and myosin II was shown to sever actin bundle into short fragments (Medeiros et al., 2006), whereas the dendritic filopodia contains short-branched F-actin (Korobova and Svitkina, 2010), on which the mechanism of the myosin II may or may not be the same.

Myosin II exerts force directly on the actin filaments and hence may increase the F-actin flow from the tip to the base. Furthermore, myosin II is an enzyme for actin network disassembly (Haviv et al., 2008; Wilson et al., 2010). Therefore myosin II may also contribute to the retrograde flow by promoting the actin network turnover in dendritic filopodia. Coincidentally, in dendritic filopodia we found that the depolymerization rate is highest at the base, where the myosin II was most active. As dendritic filopodia transform into thin spines, the retrograde flow rate diminishes in the spine necks. This difference may stem at least partly from the differential localization of myosin II in these structures. The actin disassembly activity of myosin II may also play a role in controlling the cytoskeleton morphology. Inhibition of myosin II in mature neurons resulted in the elongation of the dendritic protrusions and the loss of the spine heads (Ryu et al., 2006). Therefore myosin II may disassemble filopodia-like structure in favor of an expansive actin network, which was corroborated by the EM finding that the base of the dendritic filopodia contains a triangle-shaped actin patch (Korobova and Svitkina, 2010). The physics of

how the myosin II reorganizes the actin network in dendrites is yet to be established.

Myosin II and dendritic filopodia motility

The high motility of dendritic filopodia is believed to be important for their function in spinogenesis (Ziv and Smith, 1996); however, the mechanism of filopodia tip fluctuation is very poorly understood, with no consensus on what is the main regulatory factor. Zhuravlev and Papoian (2009) showed computationally that a stochastic reaction model of actin polymerization and depolymerization alone cannot recapitulate the large-amplitude fluctuations observed in experiments. Instead, a fluctuation source with a slower characteristic time scale is necessary. The same authors proposed the competition between formin and capping proteins as a source of the fluctuation. This prediction has not been experimentally verified. Our data point to the importance of myosin II in regulating dendritic filopodia tip fluctuations. Myosin II forces can fluctuate in dendritic filopodia due to either the stochastic binding and unbinding of myosin to actin filaments or to the stochastic phosphorylation and dephosphorylation of myosin light chain. Fluctuations in myosin activities will drive variations in F-actin flow rates, which were indeed observed in our data. Further testing of these ideas requires quantitative modeling of the biomechanical process, which will be one of the emphases of the future study.

A related question is why the filopodia did not grow appreciably under myosin inhibition. Presumably, protrusion rate would increase when retrograde flow rate decreased; however, this was not observed in our experiment, at least with short-term myosin inhibition (<:30 min). One possible explanation is that overall actin turnover rate was reduced upon myosin inhibition. Myosin inhibition reduces myosin-dependent F-actin disassembly (Haviv et al., 2008; Wilson et al., 2010) and thus may reduce the concentration of the local pool of G-actin molecules, which, in turn, will negatively affect the polymerization rate. This effect may contribute to both the slowdown of the F-actin retrograde flow and the tip growth rate and motility.

MATERIALS AND METHODS

Cell culture

Hippocampal neuron cultures were prepared from E18 rat (Sprague Dawley) embryos according to standard procedure (Tatavarty et al., 2009). Cells were plated at 20,000–30,000 cells/ml on glass-bottom culture dishes that were thoroughly cleaned by sonicating sequentially in 10% HCl, 20% NaOH, and Millipore water and coated with poly-L-lysine (Sigma-Aldrich, St. Louis, MO) overnight before use. For protein expression, cells were transfected with the corresponding DNA constructs 1 d before the imaging experiment using Lipofectamine 2000 (Invitrogen, Carlsbad, CA) following manufacturer's protocol, except for measuring F-actin flow in the dendritic filopodia of young neurons, for which cells were transfected by nucleofection (Amaxa Biosystems, Lonza, Cologne, Germany) with plasmid DNA (1–4 μg). Cell cultures were maintained for up to 25 DIV in Neurobasal medium supplemented with B27. Images were taken between DIV 9 and 16.

Chemicals and plasmids

Blebbistatin and ML7 were purchased from Calbiochem (San Diego, CA). Blebbistatin was used at 25 μM final concentration, and ML7 was used at 10 μM final concentration. Cytochalasin D was purchased from Sigma-Aldrich and used at 20 ng/ml final concentration.

For imaging F-actin dynamics, cells were transfected with a DNA vector expressing Eos-actin, which has been described previously (Tatavarty et al., 2009). For imaging dendritic filopodia mobility, cells were transfected with MyrGFP (a gift from R. Mains, University of Connecticut Health Center, Farmington, CT), a vector expressing enhanced GFP mutant carrying a myristoylation signal peptide linked to its N-terminal. Constructs for expressing wtRac1 and dnRac1(T17N) under the constitutive cytomegalovirus promoter were gifts from Yi Wu (University of Connecticut Health Center). To express Eos-MLC fusion, a Gateway cassette (Invitrogen) was inserted to the C-terminal of the tdEos sequence (a gift from J. Wiedenmann, University of Ulm), which converted the original vector into a Gateway vector. An entry clone of the myosin regulatory light chain, Mlrc2, was purchased from Open Biosystems (Thermo Biosystems, Huntsville, AL). The Mlrc2 sequence was then subcloned into the Eos Gateway vector using the LR clonase (Invitrogen) following the manufacturer's procedure to produce the Eos-MLC fusion construct.

Microscopy and image analysis

Methods for single-molecule tracking of F-actin and analysis of images were described previously (Tatavarty et al., 2009). Briefly, a modified epifluorescence microscope (Olympus IX81; Olympus, Tokyo, Japan) equipped with 60× microscope objective (numerical aperture, 1.45; Olympus) and a thermoelectric-cooled, electron-multiplying charge-coupled device camera (PhotonMax; Roper Scientific, Trenton, NJ) was used to image single F-actin molecules. A 405-nm diode laser (Cube laser system; Coherent, Santa Clara, CA) was the light source for photoactivation. The green fluorescence of unactivated EosFP is excited with the 488-nm laser line from an argon ion laser (CVI Melles Griot, Albuquerque, NM). Activated single molecules were imaged with a 532-nm, diode-pumped solid-state diode laser (Lambda Photometrics, Harpenden, United Kingdom). To study F-actin flow, we acquired time-lapse images at either 1 or 0.5 frame/s with 400-ms exposure for each image. Image acquisition software was built on top of the μManager platform (http://micromanager.org).

FRAP measurements were carried out on the confocal microscope (Zeiss) using the 488-nm laser for excitation and a standard GFP filter set. Cells were transfected to express Eos-actin and used without performing any photoactivation. The photobleaching lasted for 2 s. The recovery of fluorescence is followed at 4-s time-lapse interval. The experimental results were fitted with either a single-exponential decay model (for the integrated intensity signal) or a discretized version of Eq. 1 with the Crank–Nicolson method (for quantifying polymerization kinetics at different subregions).

For immunofluorescence microscopy, neurons were fixed with 4% paraformaldehyde for 15 min. Blocking was done for 1 h at room temperature in 10% normal goat serum with 0.1% Triton-X prepared in 1× phosphate-buffered saline (PBS). Cells were labeled with primary antibody against the phosphorylated (Ser-19) light chain of myosin II (Cell Signaling Technology, Beverly, MA) diluted at 1:75 in a solution of 2% normal goat serum in 1× PBS (overnight) and again with anti-rabbit Alexa Fluor 647 (Molecular Probes, Invitrogen) diluted at 1:2000 in 1× PBS. After PBS washes, the cells were imaged in a Zeiss LSM ConfoCor 3 microscope with 40× water immersion objective (Zeiss, Jena, Germany).

To quantify filopodia tip motility, were located the tip positions manually in ImageJ (National Institutes of Health, Bethesda, MD) by finding the first pixel along the filopodia whose fluorescence intensity drops to less than one-half of the filopodia shaft. The coordinates of the pixels were first stored in the selection manager before eventually being exported as a text file. A Matlab (MathWorks, Natick, MA) script imported the text file into a Matlab environment, calculated the distances between each pairs of tip positions separated by 2 min, and compiled the histogram.

REFERENCES

Arellano JI (2007). Ultrastructure of dendritic spines: correlation between synaptic and spine morphologies. Front Neurosci 1, 131–143.

Calabrese B, Wilson MS, Halpain S (2006). Development and regulation of dendritic spine synapses. Physiology 21, 38–47.

Cingolani LA, Goda Y (2008). Actin in action: the interplay between the actin cytoskeleton and synaptic efficacy. Nat Rev Neurosci 9, 344–356.

Deshpande VS, Mrksich M, McMeeking RM, Evans AG (2008). A bio-mechanical model for coupling cell contractility with focal adhesion formation. J Mech Phys Solids 56, 1484–1510.

Dickson RM, Cubitt AB, Tsien RY, Moerner WE (1997). On/off blinking and switching behaviour of single molecules of green fluorescent protein. Nature 388, 355–358.

Ethell IM, Pasquale EB (2005). Molecular mechanisms of dendritic spine development and remodeling. Prog Neurobiol 75, 161–205.

Frost NA, Shroff H, Kong H, Betzig E, Blanpied TA (2010). Single-molecule discrimination of discrete perisynaptic and distributed sites of actin filament assembly within dendritic spines. Neuron 67, 86–99.

Halpain S (2000). Actin and the agile spine: how and why do dendritic spines dance? Trends Neurosci 23, 141–146.

Harris KM, Jensen FE, Tsao B (1992). Three-dimensional structure of dendritic spines and synapses in rat hippocampus (CA1) at postnatal day 15 and adult ages: implications for the maturation of synaptic physiology and long-term potentiation. J Neurosci 12, 2685–2705.

Haviv L, Gillo D, Backouche F, Bernheim-Groswasser A (2008). A cytoskeletal demolition worker: myosin II acts as an actin depolymerization agent. J Mol Biol 375, 325–330.

Honkura N, Matsuzaki M, Noguchi J, Ellis-Davies GCR, Kasai H (2008). The subspine organization of actin fibers regulates the structure and plasticity of dendritic spines. Neuron 57, 719–729.

Hotulainen P, Hoogenraad CC (2010). Actin in dendritic spines: connecting dynamics to function. J Cell Biol 189, 619–629.

Hotulainen P, Llano O, Smirnov S, Tanhuanpää K, Faix J, Rivera C, Lappalainen P (2009). Defining mechanisms of actin polymerization and depolymerization during dendritic spine morphogenesis. J Cell Biol 185, 323–339.

Irwin SA, Galvez R, Greenough WT (2000). Dendritic spine structural anomalies in fragile-X mental retardation syndrome. Cerebral Cortex 10, 1038–1044.

Kawamura K et al. (2004). N-WASP and WAVE2 acting downstream of phosphatidylinositol 3-kinase are required for myogenic cell migration induced by hepatocyte growth factor. J Biol Chem 279, 54862–54871.

Korobova F, Svitkina T (2010). Molecular architecture of synaptic actin cytoskeleton in hippocampal neurons reveals a mechanism of dendritic spine morphogenesis. Mol Biol Cell 21, 165–176.

Lin CH, Thompson CA, Forscher P (1994). Cytoskeletal reorganization underlying growth cone motility. Curr Opin Neurobiol 4, 640–647.

Makishima M, Honma Y, Hozumi M, Sampi K, Hattori M, Motoyoshi K (1991). Induction of differentiation of human leukemia cells by inhibitors of myosin light chain kinase. FEBS Lett 287, 175–177.

Manley S, Gillette JM, Patterson GH, Shroff H, Hess HF, Betzig E, Lippincott-Schwartz J (2008). High-density mapping of single-molecule trajectories with photoactivated localization microscopy. Nat Methods 5, 155–157.

Medeiros NA, Burnette DT, Forscher P (2006). Myosin II functions in actin-bundle turnover in neuronal growth cones. Nat Cell Biol 8, 216–226.

Neuhoff H, Sassoè-Pognetto M, Panzanelli P, Maas C, Witke W, Kneussel M (2004). The actin-binding protein profilin I is localized at synaptic sites in an activity-regulated manner. Eur J Neurosci 21, 15–25.

Nimchinsky EA, Sabatini BL, Svoboda K (2002). Structure and function of dendritic spines. Annu Rev Physiol 64, 313–353.

Niu L, Yu J (2008). Investigating intracellular dynamics of FtsZ cytoskeleton with photoactivation single-molecule tracking. Biophys J 95, 2009–2016.

Oray S, Majewska A, Sur M (2006). Effects of synaptic activity on dendritic spine motility of developing cortical layer V pyramidal neurons. Cerebral Cortex 16, 730–741.

Pollard TD, Borisy GG (2003). Cellular motility driven by assembly and disassembly of actin filaments. Cell 112, 453–465.

Racz B, Weinberg RJ (2004). The subcellular organization of cortactin in hippocampus. J Neurosci 24, 10310–10317.

Racz B, Weinberg RJ (2006). Spatial organization of cofilin in dendritic spines. Neuroscience 138, 447–456.

Rex CS et al. (2010). Myosin IIb regulates actin dynamics during synaptic plasticity and memory formation. Neuron 67, 603–617.

Ryu J, Liu L, Wong TP, Wu DC, Burette A, Weinberg R, Wang YT, Sheng M (2006). A Critical role for myosin IIB in dendritic spine morphology and synaptic function. Neuron 49, 175–182.

Segal M (1995). Morphological alterations in dendritic spines of rat hippocampal neurons exposed to N-methyl-aspartate. Neurosci Lett 193, 73–76.

Star EN, Kwiatkowski DJ, Murthy VN (2002). Rapid turnover of actin in dendritic spines and its regulation by activity. Nat Neurosci 5, 239–246.

Takahashi H, Sekino Y, Tanaka S, Mizui T, Kishi S, Shirao T (2003). Drebrin-dependent actin clustering in dendritic filopodia governs synaptic targeting of postsynaptic density-95 and dendritic spine morphogenesis. J Neurosci 23, 6586–6595.

Tashiro A, Yuste R (2004). Regulation of dendritic spine motility and stability by Rac1 and Rho kinase: evidence for two forms of spine motility. Mol Cell Neurosci 26, 429–440.

Tatavarty V, Kim E-J, Rodionov V, Yu J (2009). Investigating sub-spine actin dynamics in rat hippocampal neurons with super-resolution optical imaging. PLoS ONE 4, e7724.

Theriot JA, Mitchison TJ (1992). Comparison of actin and cell surface dynamics in motile fibroblasts. J Cell Biol 119, 367–377.

Ward ME, Wu JY, Rao Y (2004). Visualization of spatially and temporally regulated N-WASP activity during cytoskeletal reorganization in living cells. Proc Natl Acad Sci USA 101, 970–974.

Wilson CA, Tsuchida MA, Allen GM, Barnhart EL, Applegate KT, Yam PT, Ji L, Keren K, Danuser G, Theriot JA (2010). Myosin II contributes to cell-scale actin network treadmilling through network disassembly. Nature 465, 373–377.

Yoshihara Y, De Roo M, Muller D (2009). Dendritic spine formation and stabilization. Curr Opin Neurobiol 19, 146–153.

Yuste R, Bonhoeffer T (2001). Morphological changes in dendritic spines associated with long-term synaptic plasticity. Annu Rev Neurosci 24, 1071–1089.

Zhang H, Webb DJ, Asmussen H, Niu S, Horwitz AF (2005). A GIT1/PIX/Rac/PAK signaling module regulates spine morphogenesis and synapse formation through MLC. J Neurosci 25, 3379–3388.

Zhuravlev PI, Papoian GA (2009). Molecular noise of capping protein binding induces macroscopic instability in filopodial dynamics. Proc Natl Acad Sci USA 106, 11570–11575.

Ziv NE, Smith SJ (1996). Evidence for a role of dendritic filopodia in synaptogenesis and spine formation. Neuron 17, 91–102.